Molecular Dynamics Simulations of Arp2/3 Complex Activation

Paul Dalhaimer[†] and Thomas D. Pollard[†‡*]
[†]Departments of Molecular Cellular and Developmental Biology, and [‡]Departments of Molecular Biophysics and Biochemistry, and Cell Biology, Yale University, New Haven, Connecticut

ABSTRACT Actin-related protein 2 and 3 (Arp2/3) complex forms a dendritic network of actin filaments during endocytosis and cellular locomotion by nucleating branches on the sides of preexisting actin filaments. Reconstructions of electron tomograms of branch junctions show how Arp2/3 complex anchors the branch, with Arp2 and Arp3 serving as the first two subunits of the branch. Our aim was to characterize the massive conformational change that moves Arp2 ~30 Å from its position in crystal structures of inactive Arp2/3 complex to its position in branch junctions. Starting with the inactive crystal structure, we used atomistic-scale molecular dynamics simulations to drive Arp2 toward the position observed in branch junctions. When we applied forces to Arp2 while restraining Arp3, one block of structure (Arp2, subunit ARPC1, the globular domain of ARPC4 and ARPC5) rotated counterclockwise by 30° around a pivot point in an α-helix of ARPC4 (Glu^{81}-Asn^{100}) to align Arp2 next to Arp3 in a second block of structure including ARPC3 and the globular domains of ARPC2. This active structure buried more surface area than the inactive conformation. The complex was stable in all simulations. In most simulations, collisions of subdomain 2 of Arp2 with Arp3 impeded the movement of Arp2.

INTRODUCTION

Actin-related protein (Arp) 2/3 complex is a key part of the actin cytoskeleton in most eukaryotic organisms (1). The complex consists of seven subunits including Arp2 and Arp3 (and Fig. S1 in the Supporting Material) (2). During the formation of an actin filament branch, Arp2/3 complex binds adaptor proteins called nucleation-promoting factors (NPFs), a preexisting actin filament and an actin monomer leading to the growth of a daughter filament on the side of the mother filament (3,4). It is not clear how these entities coordinate on the atomistic scale during branch formation.

Given the structural similarity between actin and Arps, it has been assumed (2,5) that branch formation involves Arp2 and Arp3 coming together at the base of the daughter filament like two subunits in an actin filament (6,7). Docking crystal structures into reconstructions of electron tomograms of branch junctions at ~25 Å resolution confirmed this arrangement of the Arp2 (5).

However, crystal structures of inactive Arp2/3 complex without NPFs or actin show the Arps separated by ~30 Å relative to the branch junction model, so a large conformational change is required to bring the Arps close enough together to initiate a branch (2,8,9). Electron microscopy (EM) established the overall shapes and positions of the Arps in the branch junction, but not the internal conformational changes associated with activation (5). In those models, the two Arps are arranged next to each other like two successive subunits along the short pitch of an actin filament, but the model was made by fitting pieces of the crystal structure into the EM reconstructions. Arp2 was detached from its neighbors and transferred next to Arp3 without taking its interactions with neighbors into account. Other models based on small angle x-ray scattering data provided additional information regarding interactions of the VCA domain of activator N-WASp and an actin monomer with Arp2/3 complex, but this model also lacks information about the conformations of each subunit (10). Therefore, alternative methods were needed to test the hypothesis that the subunits of the complex can rearrange to allow the Arps to come together like subunits in an actin filament and to characterize how the internal structure of the complex adjusts during the transition from the inactive to the active state.

Our molecular dynamics (MD) approach allows us to maintain the contacts between Arp2 and its neighbors during the transition from the inactive conformation to conformations with Arp2 in the short pitch position. This approach produces a more physically realistic transition and final structure.

We used atomistic-scale MD simulations to study the transition of Arp2/3 complex from its inactive state to the proposed active conformation. We applied an overstretched springlike force to subdomains 3 and 4 of Arp2 with the other end of the spring at the proposed active position of these subdomains next to Arp3. Only the beginning and end points were defined in the equation. Interactions of Arp2 with the other subunits in the complex determined the path taken by Arp2 between those two points. Application of a restraining force to a subset of the atoms of Arp3 avoided convection of the complex. As the spring relaxed over computationally accessible timescales, a 30° rotation of Arp2, ARPC1, ARPC5, and most of ARPC4 allowed Arp2 to move within a few Ångstroms of the target position.

Submitted May 13, 2010, and accepted for publication August 12, 2010.

*Correspondence: thomas.pollard@yale.edu

Paul Dalhaimer's present address is Department of Chemical and Biomolecular Engineering, University of Tennessee, Knoxville, TN.

Editor: Yale E. Goldman.

0006-3495/10/10/2568/9 $2.00

doi: 10.1016/j.bpj.2010.08.027

For most of the runs, a bumper-helix on Arp3 seemed to impose the main resistance to Arp2 assuming exactly the position along a short-pitch actin helix. However, in one of 12 simulations the inherent flexibility of subdomains 1 and 2 of Arp2 allowed Arp2 to avoid this barrier and to move closer to the target position than the other runs. This repositioning of Arp2 and the other subunits increased the buried surface within the complex.

METHODS

Starting crystal structures

The crystal structure of bovine Arp2/3 complex in its inactive, ATP-bound state (PDB accession code 1TYQ from Nolen et al. (8)) was the starting point for our simulations. The following residues were missing from the density and modeled using Swiss-PDB Viewer (11): Arp2 (1–142 and 351–394), Arp3 (40–51 and 354–359), ARPC1 (289–318), ARPC2 (209–216 and 283–300), ARPC3 (151–178), and ARPC5 (1–10 and 28–34). We modeled Arp2 subdomains 1 and 2 based on the ATP-actin structure 1NWK, because Arp2 and actin have higher sequence similarity than Arp2 and Arp3. Residues Thr^{283}-Arg^{300} of ARPC2 were missing from the density of the starting crystal structure, so they were modeled as an α-helix (8). A kink arises in the helix when these residues were modeled with Swiss-PDB Viewer. This discontinuity in secondary structure at Pro^{282} was required to avoid a steric clash with ARPC1. The floppy N-terminus of ARPC5 was modeled as a linear polypeptide chain.

Equilibration and production runs

We used the software package VMD (12) to surround Arp2/3 complex with a box of explicit water molecules (TIP3 model (13)) with 10 Å padding in each direction. The final solvated system contained ~250,000 atoms. The charge of the calcium ion was adjusted to 1.2 (14). The complex was equilibrated in this solvent as described in Dalhaimer et al. (14) using the NAMD 2.6 software package (15). After equilibration, the complex was simulated for 10 ns at 1 atm and 37°C (constant-NPT ensemble). The data from the long computations of Arp2/3 complex of Pfaendtner et al. (16) dictate a ~10-ns equilibration. Simulations were tested on a lab 10-processor PowerEdge SC 1425 cluster (Dell, Round Rock, TX) and subsequently run across 256-Xeon CPU cores (Intel, Santa Clara, CA). Production runs clocked at ~2 ns per day. Molecular graphics images were produced using the UCSF CHIMERA package from the Resource for Biocomputing, Visualization and Informatics at the University of California, San Francisco (17). All root mean-square deviation (RMSD) calculations were performed using the Needleman-Wunsch alignment algorithm in UCSF CHIMERA. Surface areas were calculated using the freely available MSMS package (18).

RESULTS

Molecular dynamics methodology

We used the software package NAMD to study conformational changes that take place in Arp2/3 complex when Arp2 moves from its position in the crystal structure of the inactive complex (Fig. 1 *A*) toward the position observed in EM reconstructions of branch junctions where Arp2 and Arp3 are in a short-pitch helical conformation (2,5,10). To determine the target position of Arp2 in this model we overlaid an actin subunit of the Holmes filament model (6) with Arp3 and placed Arp2 in the position occupied by the next actin subunit along the short-pitch helix (Fig. 1 *B*). We then calculated the average position of the C^{α} values of subdomains 3 and 4 of Arp2 (r_{active}). We modified the source code of NAMD (15) so that a springlike energy of the form $E = k\,(r_{active}\text{-}r_{current})^2$ could be applied to the average position of the C^{α} values of subdomains 3 and 4 of Arp2 ($r_{current}$) driving them toward the active Arp2 position (r_{active}) (Fig. 1 *C*). The spring was overstretched when Arp2 was not in the short-pitch helical conformation with Arp3. The force applied to Arp2 was tuned by changing the spring constant, k. During simulations, the value of (r_{active}-$r_{current}$) converged toward zero as subdomains 3 and 4 of Arp2 approached their target. We did not apply forces directly to subdomains 1 and 2 of Arp2, because they do not have density in crystal structures of Arp2/3 complex except in glutaraldehyde crosslinked crystals where only the P1 loop has density (PDB accession code 2P9K; Nolen and Pollard (9)).

Even with relatively high forces applied to the Arps, the thermal energy of the system was high enough (37°C) for slight movements of all the atoms to alter the final conformation slightly. Thus, we ran five simulations with the same forces to determine whether the outcomes were consistent or variable.

Atomistic-scale molecular dynamics simulations of inactive Arp2/3 complex have given insight into the behavior of

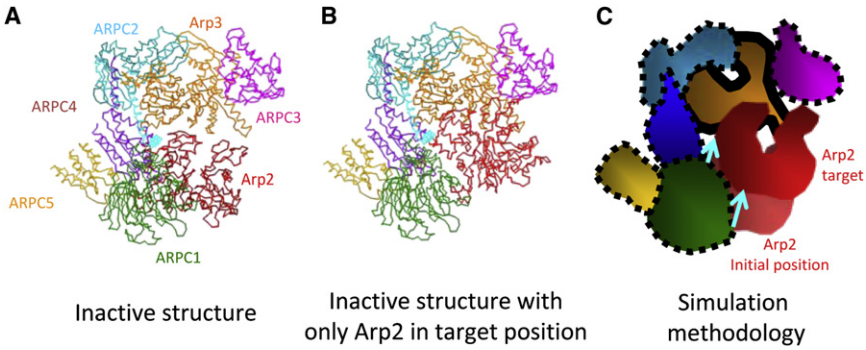

FIGURE 1 Simulation methodology. (*A*) Backbone trace of the starting crystal structure of inactive bovine Arp2/3 complex with ATP bound to both Arp2 and Arp3 (PDB accession code 1TYQ). (*B*) Arp2 and Arp3 arranged as two consecutive subunits in a short-pitch helix of an actin filament. Only Arp2 was moved in the crystal structure. (*C*) Cartoon of the simulation methodology. The force of an overstretched spring is applied between subdomains 3 and 4 of Arp2 in the inactive position and the target position next to Arp3. The spring is relaxed when the average position of the C^{α} values of subdomains 3 and 4 of Arp2 are in the target position. The C^{α} values of subdomains 1, 2, and 4 of Arp3 (*bold outline*) are restrained in a harmonic potential.

the nucleotide-binding clefts of the Arps (16). These simulations also uncovered regions of the complex that can be grouped together to give a coarse-grained model of the inactive complex. Their simulations, which ran for tens of nanoseconds, showed that the inactive complex exhibits oscillatory movement in key regions such as the nucleotide-binding clefts of the Arps on timescales of ~10 ns (16). Thus, we equilibrated Arp2/3 complex for 10 ns where no external forces were applied to the Arps. The resulting 10-ns conformation was qualitatively similar to that of Pfaendtner et al. (16) and was used as the starting point for our studies of the activation of the complex (illustrated by Fig. S2).

We ran the applied force simulations for 4 ns (from 10 to 14 ns) with k values spanning more than an order of magnitude from $k_{0.5}$ (14 kcal/mol/Å^2) to k_{10} (280 kcal/mol/Å^2) with intermediate values of $k = k_{1,1.5,2,4,6,8}$. The 12 simulations included five runs with $k = k_6$ to determine the variance between trajectories with one force. We restrained in a harmonic potential but did not fix the C$^\alpha$ values of subdomains 1, 2, and 4 of Arp3 to avoid convection of the entire complex during application of forces to Arp2. We did not restrain subdomain 3 of Arp3 so that we could observe interactions between this subdomain and Arp2. In another simulation starting from one of the 14 ns $k = k_6$ conformations, we turned off the force applied to Arp2 ($k = 0$) for 4 ns (14–18 ns) and subsequently turned off the restraints on Arp3 for the last 4 ns of this simulation (18–22 ns).

Comparison of 12 separate molecular dynamics simulations

We applied a range of springlike forces to the C$^\alpha$ values of subdomains 3 and 4 of Arp2, which moved Arp2 and associated subunits toward Arp3 (Fig. 2 *A*). Simulations with spring constants $k \geq k_4$ all moved the center of subdomains 3 and 4 of Arp2 within ~1 Å of the target position in <2 ns (Fig. 2 *A* and Movie S1 in the Supporting Material), although the behavior of Arp2 subdomains 1 and 2 differed, as elaborated upon below. After 4 ns of simulation at lower forces ($k < k_4$), subdomains 3 and 4 of Arp2 were either still moving slowly or stalled, situated >2 Å from the target position. This stall implies an energy barrier that must be overcome during branch formation, possibly by conformational changes associated with binding of NPFs and/or the mother filament.

In all 12 simulations, the movement of Arp2 toward its target position revealed that the complex had three dynamic entities (Fig. 2 *B*). Block 1 consisted of Arp3, the two globular domains of ARPC2 and all of ARPC3 (Fig. 2 *B*). Block 2 connecting the other two blocks consisted of the C-terminal α-helices of ARPC2 (Phe^{247}-Arg^{300}) and ARPC4 (Lys^{128}-Phe^{168}) (Fig. 2 *B*). Block 3 was composed of Arp2, ARPC1, ARPC5, and the globular domain of ARPC4 (Fig. 2 *B*).

The main concerted motion of the complex after the forced movement of Arp2 was a ~30° counterclockwise rotation of block 3 around an axis through the center of the β-propeller of ARPC1 as viewed from the bottom of

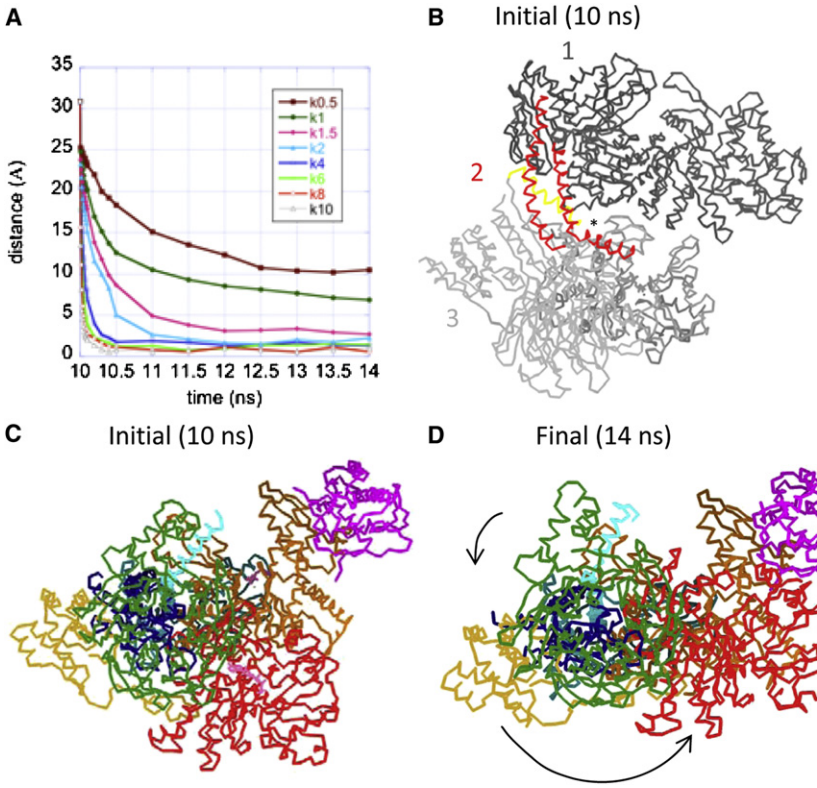

FIGURE 2 MD simulations with application of directional forces between the C$^\alpha$ values of subdomains 3 and 4 of Arp2 in the inactive position and the target position next to Arp3 while restraining the movements of the C$^\alpha$ values of Arp3 subdomains 1, 2, and 4. (*A*) Plot of the distance between the average position of the C$^\alpha$ atoms of subdomains 3 and 4 of Arp2 in the inactive and the target positions over 4 ns of simulation time for eight of the 12 different values of the spring constants: $k_{0.5}$–k_{10}. Data for only one of the five $k = k_6$ simulations are plotted. (*B*) Backbone trace of the complex at 10 ns showing the three blocks of structure described in the text: blocks 1, 2, and 3. (*C* and *D*) Basal view of the complex in initial (*C*) and final (*D*) conformations for our active model with $k = k_6$.

the complex (Fig. 2, *C* and *D*, and Movie S1). Block 1 was largely static due to the restraints on the C^{α} positions of subdomains 1, 2, and 4 of Arp3 that limited the overall displacements of the globular domains of ARPC2 and all of ARPC3.

Three parts of block 2 moved during the forced translation of Arp2:

1. A flexible joint in the long α-helix of ARPC2 (noted by an *asterisk* in Fig. 2 *B*) allowed different motions of the two halves of the helix as block 2 adapted to the path taken by block 3. The proximal part of the ARPC2 helix (Lys^{275}-Ala^{280}) moved toward the Arp2 trajectory due to interactions with the globular domain of ARPC4. The distal part of the ARPC2 helix (Thr^{283}-Arg^{300}) was largely fixed relative to block 3 by interactions with residues Asp^{306}-Ala^{319} of ARPC1. Consequently the distal helix rotated with block 3 as a result of the main thrust of ARPC4's response to the translation of Arp2 (Movie S1).
2. The helix Glu^{81}-Phe^{101} of ARPC4 (Fig. 2 *B*) pivoted in response to the movement of Arp2 due to persistent interactions with the two helices comprising block 2. This pivot-helix of ARPC4 moved into a gap (filled with explicit water in the inactive complex) between the backside of ARPC4 and the other subunits. The C-terminal helix of ARPC4 (Lys^{128}-Phe^{168}) moved in tandem with the C-terminal helix of ARPC2 (Movie S1).
3. The forced translation of Arp2 resulted in movement of the globular domain of ARPC4, because of the strong interactions between these subunits: Pro^{311}-$Gly^{312}{}_{Arp2}$ to Val^{30}-$Lys^{35}{}_{ARPC4}$ and $Thr^{237–238}{}_{Arp2}$ to Arg^{105}-$Lys^{107}{}_{ARPC4}$ (see Fig. S3). ARPC5 was pulled along with the rest of block 3 through its connections to Arp2 and ARPC4. The motion resulting from the movement of Arp2 increased the number of contacts between ARPC4 and ARPC5, thus contributing to the stability of an active conformation. The flexibility of the extended N-terminal part of ARPC5 allowed it to remain bound to Arp2 throughout the applied force simulations. As ARPC1 rotated around the axis through its β-propeller, the contacts between $Asp^{73}{}_{ARPC1}$ and $Arg^{349}{}_{Arp2}$ stretched and broke (Movie S1). This destabilization of ARPC1 may be an artifact of the forces applied to Arp2.

Interactions between Arp2 and Arp3 during simulations

Although the major conformational changes observed during the 12 MD simulations were similar, and the final structures had much in common, they differed in one main aspect. In all but one of the simulations with $k \geq k_4$ Arp3 obstructed the movement of Arp2 owing to interactions between subdomain 2 of Arp2 (particularly Arg^{38}-Ile^{40}, Fig. 3) and the long helix projecting from subdomain 3 of Arp3 consisting of residues Asp^{330} through Ile^{368} (Fig. 3). This conserved bumper-helix is three turns longer in Arp3 than in actin. Despite further movement of subdomains 3 and 4 of Arp2 toward the target position, the collision between Arp2 and Arp3 relaxed in 11 of 12 simulations (Fig. 3*C* and *D*, and Movie S2), because the applied springlike force dropped exponentially with distance as subdomains 3 and 4 approached their target. These collisions and relaxations distorted subdomains 1 and 2 of Arp2 into conformations that were unlike any crystal structures of actin monomers, filament models, or Arp2/3 complex.

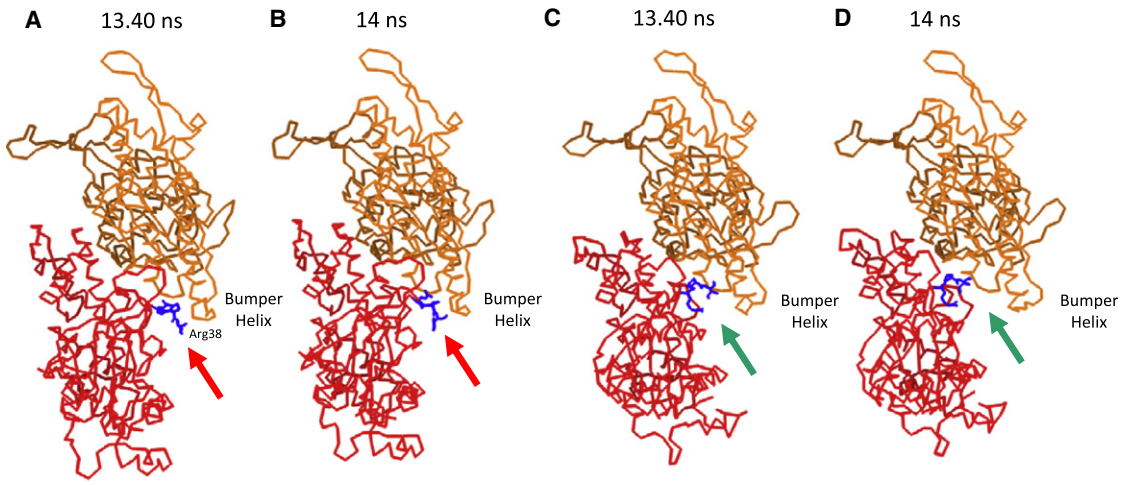

FIGURE 3 Comparison of Arp2 trajectories in two of the $k = k_6$ MD simulations. Backbone traces of subdomain 2 of Arp2 and subdomain 3 of Arp3. (*Arrows*) Region of Arp2 that must avoid Arp3 for the two subunits to form a proper short-pitch helix. (*A* and *B*) An example of a collision between Arp2 and Arp3 during one of the five $k = k_6$ simulations. Backbone traces at 13.40 ns and 14 ns show Arg^{38}-Ile^{40} getting caught under the bumper helix of Arp3. (*C* and *D*) One of the $k = k_6$ simulations where Arp2 avoids forming strong contacts with the helical bumper of Arp3 at 13.40 ns and then moves close to the target position at 14 ns. Note the actin-dimer-like gap between the Arps in panel *D*.

During one of our simulations with $k = k_6$, Arg^{38} in subdomain 2 of Arp2 avoided the bumper helix, which allowed subdomains 1 and 2 of Arp2 to move along with subdomains 3 and 4 toward the target (Fig. 3*C* and *D*, and Movie S3).

The structure at the end of this simulation seems the most realistic of our 14-ns conformations in three ways:

1. Arp2 was located next to Arp3 like two subunits of an actin filament (Fig. 3 *D*).
2. The conformation of the Arp2 subunit was similar to both the starting conformation of Arp2 and crystal structures of actin and Arp3.
3. This structure buried more surface area between several of the subunits than the other 11 models and even the inactive starting structure.

For these reasons, we present the conformation at the end of this simulation as our model of active Arp2/3 complex.

Behavior of the contacts between subunits during applied forces

The overall architecture of Arp2/3 complex was stable during forced movement of Arp2, owing to large contacts between most of the subunits. The combination of the remarkable stability of subunit contacts in block 1 (Fig. 4 *A*) with the dynamic response of block 3 exposed the centrally located ARPC4 to complicated stresses that produced a rotation around the pivot point located at the helix Glu^{81}-Phe^{101} of ARPC4 (Movie S1). These forces produced changes in buried surface area between subunits in other parts of the complex as measured by the MSMS program (18).

In the $k = k_6$ simulation where Arp2 avoided the Arp3 bumper helix, the buried surface area increased between ARPC1-ARPC2, ARPC1-ARPC4, ARPC1-ARPC5, ARPC2-ARPC4, and ARPC4-ARPC5 (Fig. 4 *A*). The surface buried between Arp2 and Arp3 in the active model was less than in the starting structure and in the 11 other 14-ns conformations. Similarly, the force on Arp2 pulled the residues at the interface

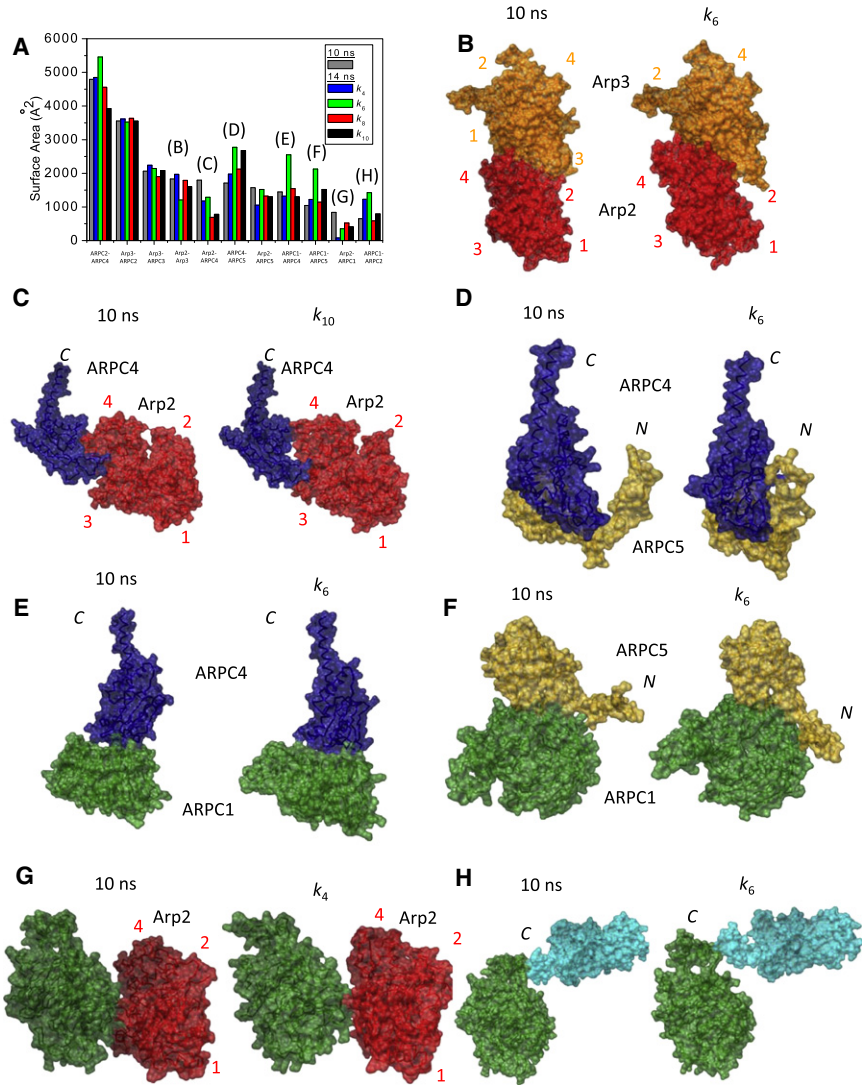

FIGURE 4 Buried surface area between pairs of contacting subunits. (*A*) Plot of the surface area between pairs of subunits in the 10-ns starting structure and at the end of the MD simulations at 14 ns with the four largest spring constants. (*B–H*) Space-filling models and backbone traces of the pairs of subunits that change the most in surface contact areas during the MD simulations. The $k = k_6$ subunits are of the active model. (*B*) Arp2-Arp3, (*C*) Arp2-ARPC4, (*D*) ARPC4-ARPC5, (*E*) ARPC1-ARPC4, (*F*) ARPC1-ARPC5, (*G*) Arp2-ARPC1, and (*H*) ARPC1-ARPC2.

of Arp2 and ARPC4 in opposite directions, so the amount of buried interface between them decreased as these subunits separated (Fig. 4*A* and *C*).

On the other hand, as the Arps aligned in the active conformation, the buried surface area increased between ARPC4 and ARPC5 (Fig. 4 *D*) and also between ARPC1 and ARPC4 (Fig. 4 *E*). The N-terminus of ARPC5 swung down and formed a tight complex with ARPC1 (Fig. 4 *F*). Thus, the N-terminus of ARPC5 is greatly stabilized by its newly formed interactions with ARPC1 and ARPC4. In all simulations with $k \geq k_4$, ARPC1 separated from Arp2 (Fig. 4 *G*) but increased its contacts with the C-terminus of ARPC2 (Fig. 4 *H*).

The program DynDom (19) identified few dynamic domains in subunits of Arp2/3 complex in comparisons of the inactive and active conformations of Arp2/3 complex. This is because the movements of the dynamic entities are complex and best viewed by observing Movie S1, Movie S2, and Movie S3 provided in the Supporting Material. However, the DynDom program identified subdomains 1+2 and 3+4 of Arp2 as two separate dynamic entities and residues Val^{287}-Gly^{318} of ARPC1 as having overall dynamic motion different from the rest of ARPC1, as expected for residues lacking electron density in the crystal structures. The dynamics of this region of ARPC1 seem to be affected by its interaction with the C-terminus of ARPC2 (Fig. 4 *H*).

Impact of restraining subunits on the motions of other subunits

We compared simulations with restraints on the C^{α} positions of subdomains 1, 2, and 4 of Arp3 with four separate simulations with $k = k_6$ and additional restraints on either the C^{α} values of ARPC1, the C-terminus of ARPC2 (residues Ala^{280}-Arg^{300}), ARPC4 or ARPC5. The aim of these 1-ns simulations was to characterize the requirements for the large translocation of Arp2. Arp2 moved roughly the same distance with each of these restraints (Fig. S4), but subdomains 3 and 4 of Arp2 were torn apart if restraints prevented ARPC4 from following along. Restraining neighboring subunits strongly influenced the displacement of ARPC1: its overall movement dropped by 40–50% when the C-terminus of ARPC2, all of ARPC4 or all of ARPC5 were restrained (Fig. S4). The displacements of ARPC4 and ARPC5 were reduced by ~50% when the other was restrained. The movements of ARPC2, and to a lesser extent ARPC4, were widely reduced when ARPC1, ARPC4, or ARPC5 were restrained (Fig. S4). At least one restraint out of the four tested affected the displacement of the other five subunits by <10% (Fig. S4).

Repeated and extended simulation runs show complex stability

To test the stability of the active conformation produced by our simulation, we removed the force applied to subdomains 3 and 4 of Arp2 for 4 ns and thereafter also removed the restraints on subdomains 1, 2, and 4 of Arp3 for another 4 ns. If the force applied to the complex from 10 to 14 ns was excessive and the complex was in a high-energy conformation, we expected to observe large displacements from 14 to 18 ns and 18 to 22 ns.

Subunits from the conformations at 0 ns and 10 ns were individually overlaid and their RMSD values were calculated (Table S1). These values were compared to the RMSD values obtained in the same way from overlays of the individual subunits from the 10 ns and 14 ns conformations for each of the five $k = k_6$ runs (Table S1). There were no increasing trends in RMSD values between these sets of simulations. Subunits from the conformations at 14 ns and 15–22 ns were individually overlaid and their RMSD values were calculated (Table S1). Again, there was no correlation between displacement of overlaid subunits and applied force.

When the force was taken off of Arp2 in the active conformation, the changes were minor over the subsequent four nanoseconds of simulation. Subdomains 3 and 4 of Arp2 moved ~2 Å in the general direction of its starting position in the inactive conformation (Fig. S5 *A*), and the nucleotide-binding cleft and cleft mouth of Arp2 closed slightly (Fig. S5 *B*), assuming a conformation similar to Arp3 (8,9) and ATP-actin (20) (Fig. S5 *C*).

When the forces applied to Arp2 were turned off for the simulations where Arg^{38}-Ile^{40} were caught under the bumper helix of Arp3, subdomain 2 of Arp2 was the only part of the complex that showed a noticeable adjustment with further simulation. At 15 ns with $k = 0$, subdomain 2 relaxed toward the position of subdomain 2 in the crystal structures of actin and Arp3 (Fig. S5, *D* and *E*). This relaxed position of subdomain 2 of Arp2 was similar to the position of subdomain 2 in the $k = k_6$ simulation where Arp2 did not get stuck under the bumper helix of Arp3 (Fig. 3 *D* versus Fig. S5, *D* and *E*).

DISCUSSION

Force applied to subdomains 3 and 4 of Arp2 produced 30° rotation of block 3 that moved Arp2 toward its active position next to Arp3. This rotation arises from the attachment of Arp2 to ARPC4, the persistent attachment of ARPC4 to ARPC2 and to ARPC1, and favorable interactions that formed between ARPC4 and ARPC5 during the simulations. Stable interfaces between ARPC2 and both Arp3 and ARPC4 forced the complex to pivot in the vicinity of helix Glu^{81}-Phe^{101} of ARPC4. Importantly, this rearrangement took place in a region of Arp2/3 complex that interacts with the mother filament (5). Binding to a mother filament is essential for activation of Arp2/3 complex (1,21) and mutations in this region of ARPC2 greatly affect the activity of the complex (22).

Comparisons with other models of active Arp2/3 complex

We base this discussion on the "active conformation" obtained at 14 ns of MD simulation with the spring constant $k = k_6$, where Arp2 avoided a collision with Arp3. In this simulation, subdomain 2 of Arp2 most resembled that of crystal structures of actin and Arps, and the buried surface area between subunits was on average the highest over all forces used—even compared with the starting inactive conformation after 10 ns of simulation without an applied force.

Overlays illustrate the differences between our active MD model and the EM model based on the reconstruction of electron micrographs of branch junctions (Fig. 5). Given that the methods have nothing in common, the overall features of the MD and EM models are remarkably similar

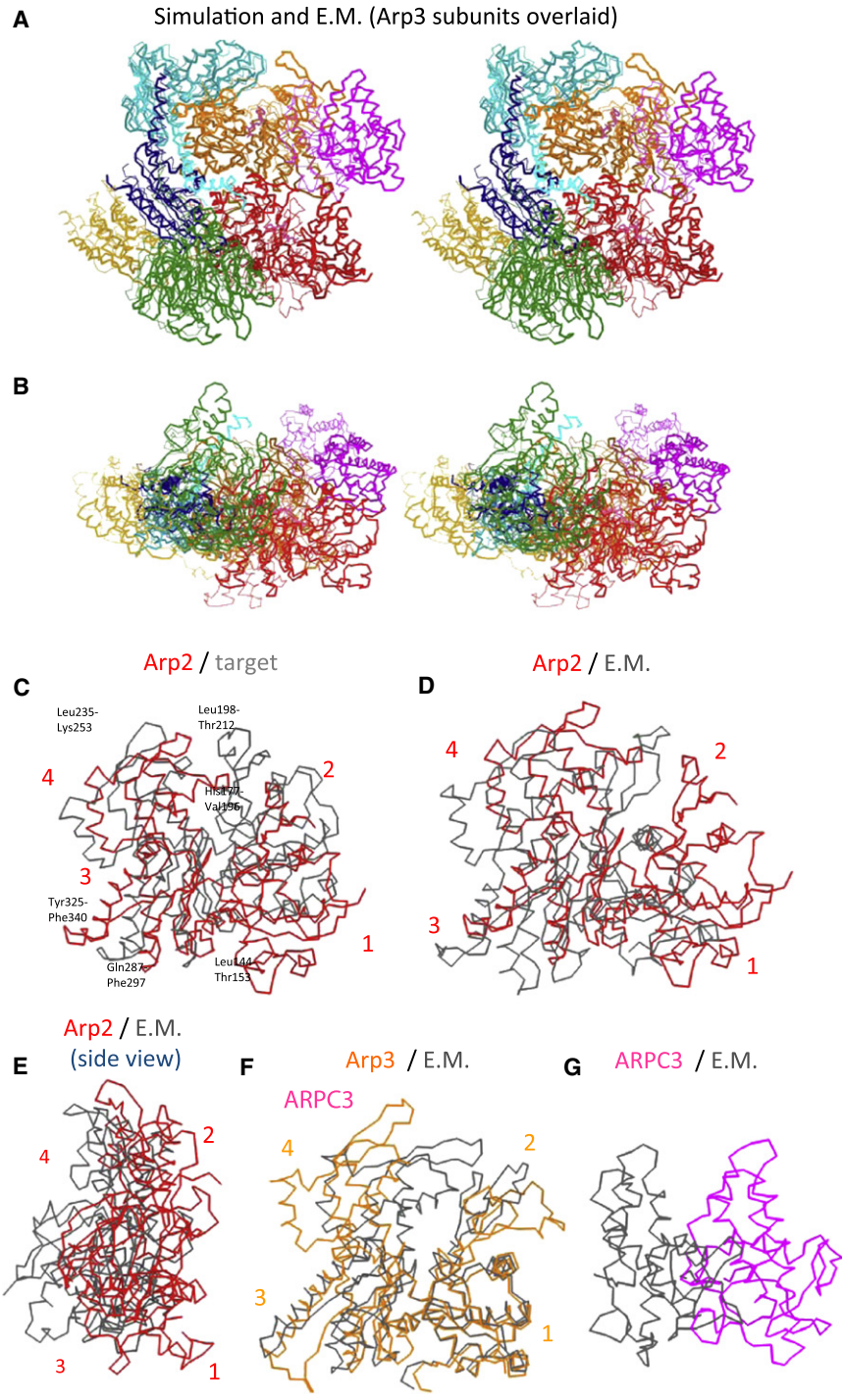

FIGURE 5 Comparison of our active MD model and the EM model. (*A* and *B*) Structures aligned by overlaying the Arp3 subunits. Stereo pairs in the (*A*) standard orientation and (*B*) from the bottom of the complex with thick lines for the backbone of the MD model and thin lines for the EM model. (*C–G*) Overlays of the backbone traces of the subunits from our active MD model with the target and the EM model. The complexes were aligned by matching the positions of the Arp3 subunits. Subunits were chosen that had the largest differences in position between the models. (*C*) Arp2 and target, (*D*) Arp2 and EM, (*E*) Arp2 and EM side view, (*F*) Arp3 and EM, and (*G*) ARPC3 and EM.

to each other and different from the inactive crystal structure. In particular, Arp2 and associated subunits in Block 3 are positioned closer to Arp3 than in the inactive complex. The two methods do not give the same result, because the MD simulations did not include interactions with the mother filament.

The main differences between the EM and MD models are the positions of Arp2, the closure of the nucleotide-binding clefts of Arp2 (Fig. S1 and Fig. S6, *B* and *C*) and Arp3 (Fig. S1 and Fig. S6 *D*), and the position of the ARPC3 subunit, which arises simply from the differences in Arp3 (Fig. S6 *E*) (Fig. S1). Fitting crystal structures of subunits into the reconstruction of the branch junction required tightly closing the nucleotide binding clefts of both Arps (see Table S2 for the cleft dimensions) and rotating the two halves of the protein flanking the nucleotide ~15°. Closure of the Arp3 cleft positioned ARPC3 inside the experimental density closer to the center of the complex than in the inactive crystal structure or our active model.

Because we do not see the Arp clefts close or the ~15° rotation of the two halves of both Arps in our simulations, interactions with nucleation promoting factors or the mother filament are most likely required for these conformational changes to take place during branch formation. The pointed ends of both Arps interact with the mother filament (5) and conformational changes of the complex by itself, as we have studied here, do not complete the activation process and allow for nucleation, which requires binding of Arp2/3 complex to a mother filament (1,21).

Mechanism of the activating conformational change

In all of our MD simulations with $k \geq k_4$, the average x, y, z position of subdomains 3 and 4 of Arp2 moved within 1 Å of its defined target position (Fig. S6 *A*), but the behavior of Arp2 subdomains 1 and 2 varied considerably. Our MD simulations revealed that the bumper helix of Arp3 is an obstacle to the movement of Arp2 into the active conformation. Even when applying force in our MD simulations, Arp2 avoided Arp3 in only one out of 12 runs, so bringing the Arps together like subunits in an actin filament has a low probability.

The key issue to be considered in further work is the source of energy to promote the conformational changes that we observed by applying force in our MD experiments. Because Arp2/3 complex is essentially inactive on its own, thermal motions alone are inadequate to produce active complex. Given that both nucleation promoting factors and a mother filament are required to initiate a daughter filament (1,21), one or both of these binding reactions may lower the activation energy to move Arp2 into juxtaposition with Arp3 complex in the active conformation. Mother filament binding is the prime candidate, because the interface with Arp2/3 complex buries >9100 Å^2 of surface area (7), including regions such as ARPC4 where conformational changes are coupled to the movement of Arp2. ARPC4 and ARPC5 interact directly with the mother filament (5,23), and the conformations of ARPC1, ARPC4, and ARPC5 change in response to the forced movement of Arp2. Thus it stands to reason that the mother filament could promote the movement of the subunits in block 3 observed to move in this work. Such a mechanism would involve force within the complex pushing Arp2 into position. Such a mechanism may produce a more favorable trajectory for Arp2 than the linear spring used in the MD simulations.

The inherent flexibility of subdomains 1 and 2 of Arp2 is probably an important factor in activation of Arp2/3 complex during interactions with nucleation promoting factors and the mother filaments. These two subdomains are likely to be highly mobile, given the lack of electron density in most crystal structures of Arp2/3 complex except for partial density in one crystal crosslinked with glutaraldehyde (2,9). Collisions of subdomain 2 with Arp3 are the main impediment to activation, but their flexibility may allow subdomain 2 to avoid a small fraction of collisions with Arp3 and allow Arp2 to reach its target as observed in our most successful MD trajectory. Additional information about the behavior of subdomains 1 and 2 will be required to obtain more satisfactory models of Arp2/3 complex activation by computational techniques.

SUPPORTING MATERIAL

Two tables, six figures, and three movies are available at http://www.biophysj.org/biophysj/supplemental/S0006-3495(10)01014-3.

The authors thank Brian Dobbins for assistance with cluster access and computations, Greg Voth for advice, and Rose Dortch for careful editing of the manuscript.

This work was supported by National Institutes of Health research grants No. GM-026338 and No. GM-066331 (to T.D.P.), Ruth Kirschstein Fellowship grant No. F32GM074504 (to P.D.), and the facilities and staff of the Yale University Faculty of Arts and Sciences High Performance Computing Center.

REFERENCES

1. Pollard, T. D. 2007. Regulation of actin filament assembly by Arp2/3 complex and formins. *Annu. Rev. Biophys. Biomol. Struct.* 36:451–477.
2. Robinson, R. C., K. Turbedsky, …, T. D. Pollard. 2001. Crystal structure of Arp2/3 complex. *Science.* 294:1679–1684.
3. Mahaffy, R. E., and T. D. Pollard. 2006. Kinetics of the formation and dissociation of actin filament branches mediated by Arp2/3 complex. *Biophys. J.* 91:3519–3528.
4. Beltzner, C. C., and T. D. Pollard. 2008. Pathway of actin filament branch formation by Arp2/3 complex. *J. Biol. Chem.* 283:7135–7144.
5. Rouiller, I., X. P. Xu, …, D. Hanein. 2008. The structural basis of actin filament branching by the Arp2/3 complex. *J. Cell Biol.* 180:887–895.
6. Holmes, K. C., D. Popp, …, W. Kabsch. 1990. Atomic model of the actin filament. *Nature.* 347:37–44.
7. Oda, T., M. Iwasa, …, A. Narita. 2009. The nature of the globular- to fibrous-actin transition. *Nature.* 457:441–445.

8. Nolen, B. J., R. S. Littlefield, and T. D. Pollard. 2004. Crystal structures of actin-related protein 2/3 complex with bound ATP or ADP. *Proc. Natl. Acad. Sci. USA.* 101:15627–15632.
9. Nolen, B. J., and T. D. Pollard. 2007. Insights into the influence of nucleotides on actin family proteins from seven structures of Arp2/3 complex. *Mol. Cell.* 26:449–457.
10. Boczkowska, M., G. Rebowski, …, R. Dominguez. 2008. X-ray scattering study of activated Arp2/3 complex with bound actin-WCA. *Structure.* 16:695–704.
11. Guex, N., and M. C. Peitsch. 1997. SWISS-MODEL and the Swiss-PDBViewer: an environment for comparative protein modeling. *Electrophoresis.* 18:2714–2723.
12. Humphrey, W., A. Dalke, and K. Schulten. 1996. VMD: visual molecular dynamics. *J. Mol. Graph.* 14:33–38, 27–28.
13. Jorgensen, W. L., J. Chandrasekhar, …, M. L. Klein. 1983. Comparison of simple potential functions for simulating liquid water. *J. Chem. Phys.* 79:926–935.
14. Dalhaimer, P., T. D. Pollard, and B. J. Nolen. 2008. Nucleotide-mediated conformational changes of monomeric actin and Arp3 studied by molecular dynamics simulations. *J. Mol. Biol.* 376:166–183.
15. Phillips, J. C., R. Braun, …, K. Schulten. 2005. Scalable molecular dynamics with NAMD. *J. Comput. Chem.* 26:1781–1802.
16. Pfaendtner, J., and G. A. Voth. 2008. Molecular dynamics simulation and coarse-grained analysis of the Arp2/3 complex. *Biophys. J.* 95:5324–5333.
17. Pettersen, E. F., T. D. Goddard, …, T. E. Ferrin. 2004. UCSF CHIMERA—a visualization system for exploratory research and analysis. 25:1605–1612.
18. Sanner, M. F., A. J. Olson, and J. C. Spehner. 1996. Reduced surface: an efficient way to compute molecular surfaces. *Biopolymers.* 38:305–320.
19. Hayward, S., and H. J. C. Berendsen. 1998. Systematic analysis of domain motions in proteins from conformational change: new results on citrate synthase and T4 lysozyme. *Proteins.* 30:144–154.
20. Graceffa, P., and R. Dominguez. 2003. Crystal structure of monomeric actin in the ATP state. Structural basis of nucleotide-dependent actin dynamics. *J. Biol. Chem.* 278:34172–34180.
21. Achard, V., J. L. Martiel, …, R. Boujemaa-Paterski. 2010. A "primer"-based mechanism underlies branched actin filament network formation and motility. *Curr. Biol.* 20:423–428.
22. Rodal, A. A., O. Sokolova, …, B. L. Goode. 2005. Conformational changes in the Arp2/3 complex leading to actin nucleation. *Nat. Struct. Mol. Biol.* 12:26–31.
23. Gournier, H., E. D. Goley, …, M. D. Welch. 2001. Reconstitution of human Arp2/3 complex reveals critical roles of individual subunits in complex structure and activity. *Mol. Cell.* 8:1041–1052.